International Journal of Progressive Sciences and Technologies (IJPSAT)
ISSN: 2509-0119.

http://ijpsat.ijsht-journals.org
Vol. 29 No. 1 October 2021, pp.590-597

Resistance Analysis for NPL Hull with Bow Variations using CFD

Latuhorte Wattimury[1] and Antoni Simanjutak[2]

[1]Department of Marine Engineering, Universitas Patimura
Maluku, Indonesia

[2]Department of Marine Engineering, Universitas Patimura
Maluku, Indonesia

Abstract—Ships must have good performance and economic value. To achieve it, optimum speed is needed with minimal engine power usage so it can increase the efficiency of fuel use. The use of engine power is closely related to the total resistance on a ship. One alternative way to reduce ship resistance is to set the shape of the bow of the ship. This research aims to obtain the resistance of ships with variations in the type of bow shape of the ship. The analysis on this research uses numerical method using CFD. Variations in the modelling using NPL with 4 variations of bow hull. Based on the results of CFD calculations, each model NPL hull is obtained, namely; Model 0 to 4. Referring to the results of the analysis, resistances of the NPL using the model 1 design is the best model for low (Fr=0.2) and high speed (Fr>0.4) and using NPL model 1 and 3 are the best for medium speed (Fr=0.25 to 0.35).

Keywords—resistance; NPL hull, bow variations, CFD.

I. Introduction

A bulbous bow is a protruding bulb at the bow of a ship just below the waterline. The bulb modifies the way the water flows around the hull, reducing drag and thus increasing speed, range, fuel efficiency, and stability. Ships with bulbous bows generally have a 12 to 15 percent better fuel efficiency than similar vessels without them [1].

Bulbous bow can help to reduce a ship's resistance and thus to save the fuel consumption up to 15%, however, it is also regarded as a threat to a struck ship in collision accidents because it may generally penetrate the side shell of the vessel, which may cause the leakage of hazardous goods. How to avoid the serious consequence of ship-to-ship collision accidents through the bulbous bow design have become a focus of ship design [2].

Bulbous bows are today commonplace in the design of ships. Although their origins are to be found before the turn of the last century, the first application appears to have been in 1912 by the US Navy. The general use in merchant applications appears to have waited until the late 1950s and early 1960s.

The basic theoretical work on their effectiveness was carried out by Wigley (1936) in which he showed that if the bulb was nearly spherical in form, then the acceleration of the flow over the surface induces a low-pressure region which can extend toward the water surface. This low-pressure region then reacts with the bow pressure wave to cancel or reduce the effect of the bow wave. The effect of the bulbous bow, therefore, is to cause a reduction, in the majority of cases, of the effective power required to propel the vessel, the effective power P_E being defined as the product of the ship resistance and the ship speed at a particular condition in the absence of the propeller. Figure 1 shows a typical example of the effect of a bulbous bow from which it can be seen that a bulb is, in general, beneficial above a certain speed and gives a penalty at low speeds. This is due to the balance between the bow pressure wave reduction effect and increase in frictional resistance caused by the presence of the bulb on the hull.

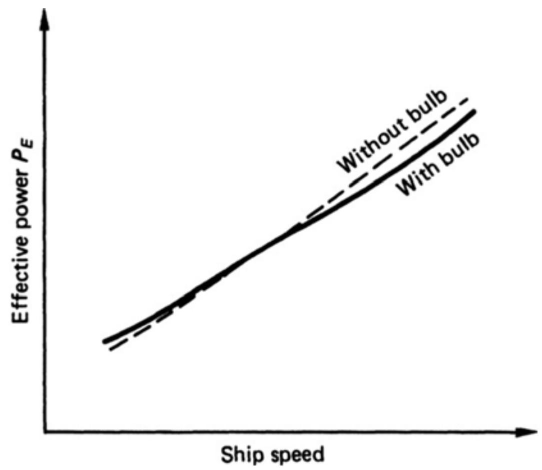

Figure 1 Influence of a bulbous bow of the effective power requirement.

Originally the bulbous bow was sized, shaped, and positioned to create a bow wave system partially cancelling out the ship's own bow wave system and reducing wave-making resistance. This applied only over a limited speed range and at the expense of resistance at other speeds. Many merchant ships operate at a steady speed for much of their lives so the bulb was designed for that speed. It was initially applied to moderate- to high-speed ships but has also been found to be beneficial in relatively slow ships such as bulk carriers, which now often have bulbous bows. The effectiveness of the bulb in the slower ships, where wave-making resistance is small, suggests the bulb reduces frictional resistance as well. This is due to the change in flow velocities over the hull and into the propeller, and the benefit is mainly in the ballast condition. Sometimes the bulb is sited well forward and it can extend beyond the fore perpendicular.

Further, the development for hull optimization was carried out using Axe-bow. It uses straight vertical sides to dampen waves from the bow, this can result in a smooth pitching motion. Basically, the Axe-bow in the extended section is empty space. The study of Axe-bow shows an increase in efficiency and a reduction in pitch acceleration, because of which ships with Axe-bow have less resistance in conventional models and reduce fuel use [3]

The Axe-bow developed by Damen Shipyard has better efficiency as well as better head sea performance with less slamming and higher speeds [4]. Damen Shipyard [5], made the delivery of the first ship, the Patrol Boat with axe-bow. The ship exhibits effective movement behavior and significantly lower drag while sailing. This provides a 20% reduction in fuel use and consequently lower emissions. Through the CFD analysis on the optimum hull, it was possible to confirm the reduction of added resistance by the reflected wave around the bow smoothly spread to the side [6].

The advantages that have been mentioned in the previous literature to reduce ship resistance, using the NPL hull with variations of bow hull. This paper discusses the bow variations of NPL hull to obtain a better resistance reduction. The main objective of the study is to analyze the resistance characteristics on a NPL Hull with four variations of bow by utilizing CFD method based on RANS (Reynolds-averaged Navier-Stokes) . Further, the bow hull effect is calculated to determine the best shape of bow hull.

II. Ship Model with Bow Variations

This research was conducted on the NPL hull with 4 variations of the bow shape with the model sizes shown in Table 1. The 4 variations of the NPL hull model in question are Model 0, namely the NPL hull model with no changes to the bow, Model 1, Model 2 and Model 3. The variation of the models are shown in Figure 2.

Table 1 Particular Dimensin of NPL Hull

	Unit	NPL Hull			
		Model 0	Model 1	Model 2	Model 3
Length over All (L_{OA})	m	1.252	1.252	1.252	1.362
Length at Water Line (L_{WL})	m	1.182	1.19	1.252	1.313
Breath (B)	m	0.168	0.168	0.168	0.168
Draft (T)	m	0.067	0.077	0.077	0.078
Heigh (H)	m	0.186	0.186	0.186	0.186
Water Surface Area (WSA)	m^2	0.181	0.188	0.201	0.215
Coefficient Block (Cb)	-m	0.338	0.283	0.273	0.262
Displasment (Δ)	kg	3.745	3.758	3.71	3.794

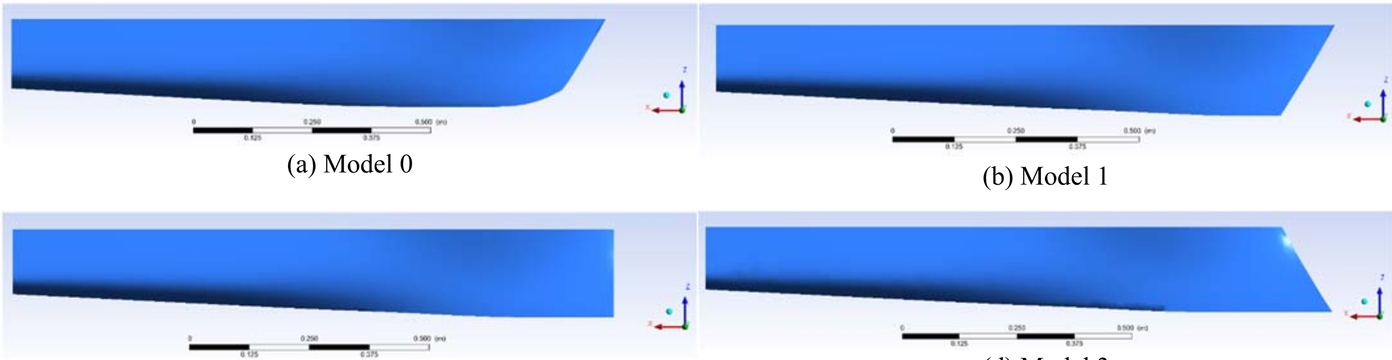

(a) Model 0

(b) Model 1

(c) Model 2

(d) Model 3

Figure 2 NPL Hull

III. METHOD

A. Governing Equation

The research methodology that will be used to solve the problem of trimaran ship is numerical simulations by applying the Computational Fluid Dynamic (CFD). The geometry configuration of the simulated model is the displacement type with symmetrical hull shown in Figure 2. Numerical simulations are carried out using the CFD model developed from the Navier-Stokes equation which is able to explain the phenomenon of flow around the hull so that the causes of the ship has high or low resistance will be acknowledged.

The choice of turbulence models is found to be very crucial in the simulation of wake fields. The turbulence model used in the current study is the SST (Shear Stress Transport) model developed by Luhulima [7] This SST model has been validated by several researchers as described in [8] with successful results. The viscous flow field is solved using RANS (Reynolds Averaged Navier-Stokes) solver implemented in ANSYS CFX. The RANS, turbulence *k-ω* and turbulence SST are shown in equations (1), (2) and (3). The RANS equation is given by:

$$\frac{\partial(\rho U)}{\partial t} + \frac{\partial}{\partial x_j}(\rho U_i U_j) = -\frac{\partial p}{\partial x_j} + \frac{\partial}{\partial x_j}(\tau_{ij} - \overline{\rho u_i u_j}) + S_M \tag{1}$$

The left hand side of equation (4) represents the change in mean momentum of fluid element to the unsteadiness in the mean flow. This change is balanced by the mean body force, the mean pressure field, the viscous stresses, and apparent stress to the fluctuating velocity field. The *k-ω* equation is expressed as:

$$\frac{\partial}{\partial t}(\rho k) + \frac{\partial}{\partial x_i}(\rho k u_i) = \frac{\partial}{\partial x_j}\left(\Gamma\omega \frac{\partial\omega}{\partial x_j}\right) + G^{\sim}k + Yk + Sk \tag{2}$$

Further, the computing and simulation of SST turbulence models applied the method as introduced by Menter [9] and [10]. Here the Menter's SST equation has the form of:

$$\frac{\partial}{\partial t}(\rho\omega) + \frac{\partial}{\partial x_i}(\rho\omega u_i) = \frac{\partial}{\partial x_j}\left(\Gamma\omega \frac{\partial\omega}{\partial x_j}\right) + G^{\sim}\omega - Y\omega + D\omega + S\omega \tag{3}$$

where $G^{\sim}k$ represents the generation of turbulence kinetic energy due to mean velocity gradients, Gω represents the generation of ω, Γk and Γω represent the effective diffusivity of k and ω, respectively. Sk and Sω are user-defined source terms. Yk and Yω represent the dissipation of k and ω due to turbulence. Dω represents the cross-diffusion term.

The SST turbulence model has been validated in a number of studies among others by Bardina [11] and [12], and is considered as the most accurate models for various flow applications. This turbulent model solves the turbulence based (*k-ω*) on walls and turbulence based (*k-ε*) on the mass flow.

B. ***Boundary Condition and Meshing***

The domain dimensions and boundary conditions are specified in Figure 3. The boundary conditions are specified as follows: the hull body is a no-slip condition is imposed on the hull surface; free-slip condition is applied to the top, side and bottom walls; symmetry condition is used for the hull centre plane; the flow velocity at inlet is defined as the tested speed; at the outlet, the hydrostatic pressure defined as a function of water level height is applied; furthermore, the initial location of the free surface is determined by defining the volume fraction function of water and air at the inlet and outlet.

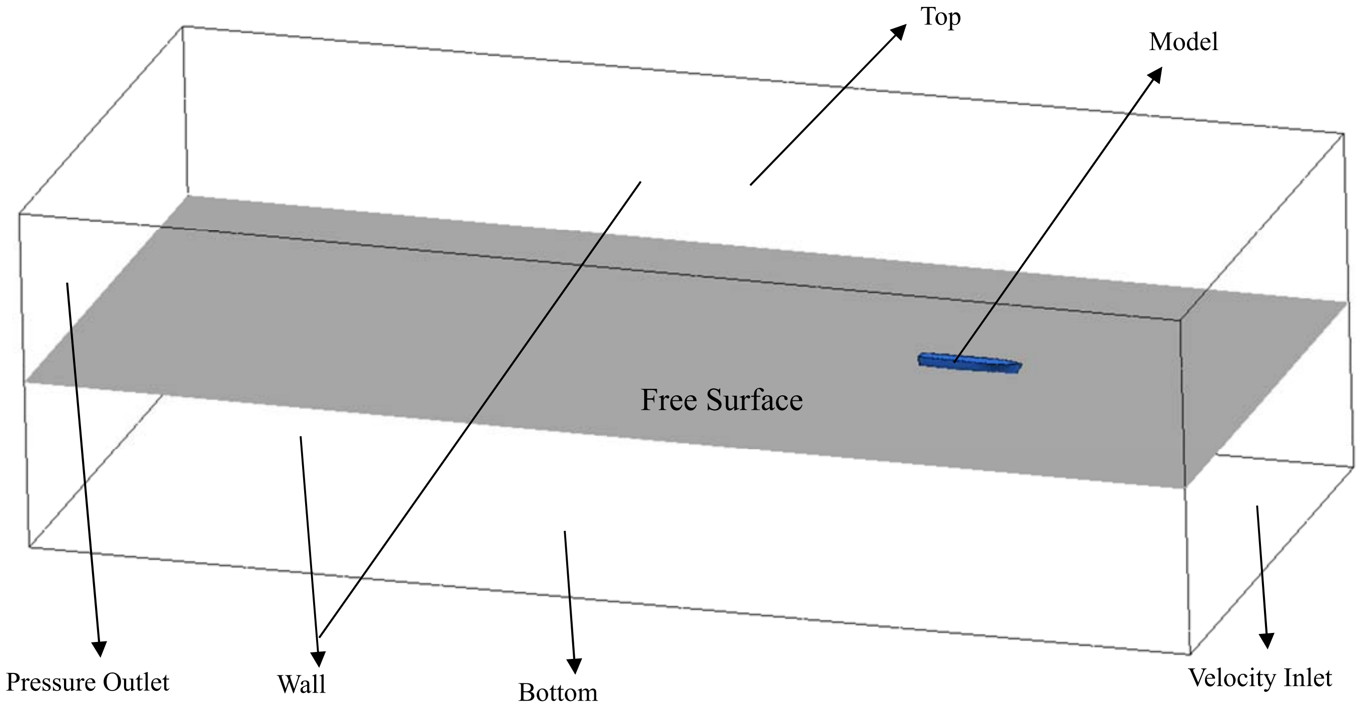

Figure 3 Boundary Condition of ship model

The mesh generation in this study is accomplished using Design Modeler. The calculation domain is discretized using structured and unstructured meshes. Considering the complex geometrical characteristics of the hull, a mesh with triangular elements is generated on the hull surface and the boundary layer is refined with prism elements created through extending the surface mesh node. The region around the boat is filled with tetrahedral elements with inflation, while in the far field, unstructured mesh with grid generation is generated for reducing the number of elements as shown Figure 4. The mesh size plays an important role in the calculation procedure, a fine mesh can always bring credible results in ANSYS CFX but at the same time increases the computational cost and time consumption due to the large element number.

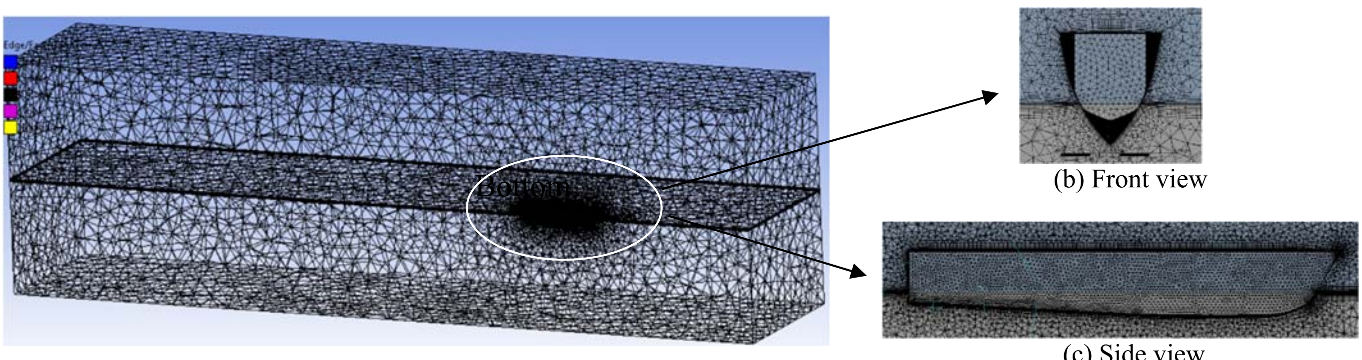

(a) Meshing Boundary (b) Front view (c) Side view

Figure 4 Meshing Model

IV. Result and Discussion

The calculation of drag is carried out on four variants of the NPL hull bow as shown in table 2, namely Model 0 (with no modifications), Model 1, Model 2, and Model 3. The calculations are carried out on four variations of the NPL hull bow. CFD simulation reveals that NPL Model 0 has the lowest resistance at low speed (Fr=0.2), with a difference of 2.6 percent from Model 1, 5.3 percent from Model 2, and 15.8 percent from Model 3. At medium speed with Fr=0.3 shows NPL Model 2 has the smallest resistance compared to others, where it it is 1.8% smaller than Model 1, 5.8% smaller than Model 0 and 9.0% smaller than Model 3. Furthermore, the NPL hull resistance at high speed with Fr = 0.65 revealed that Model 0 has the lowest resistance, with a difference of 0.6 percent from Model 2, 1.4 percent from Model 1, and 7.9 percent from Model 3. Model 2 has the most resistance, with a difference of 0.6 percent from Model 3. Figure 5 clearly illustrates that they are the most significant when compared to the others.

Table 2 Coefficient Tota Resistance of NPL Hull Variations

Fr	NPL Hull			
	Model 0	Model 1	Model 2	Model 3
0.2	0.0083	0.0085	0.0088	0.0096
0.25	0.0084	0.0081	0.0080	0.0093
0.3	0.0084	0.0081	0.0079	0.0087
0.35	0.0083	0.0082	0.0081	0.0087
0.4	0.0082	0.0083	0.0083	0.0088
0.45	0.0080	0.0082	0.0083	0.0087
0.5	0.0078	0.0081	0.0080	0.0084
0.55	0.0076	0.0079	0.0078	0.0082
0.6	0.0075	0.0077	0.0076	0.0080
0.65	0.0074	0.0077	0.0075	0.0079

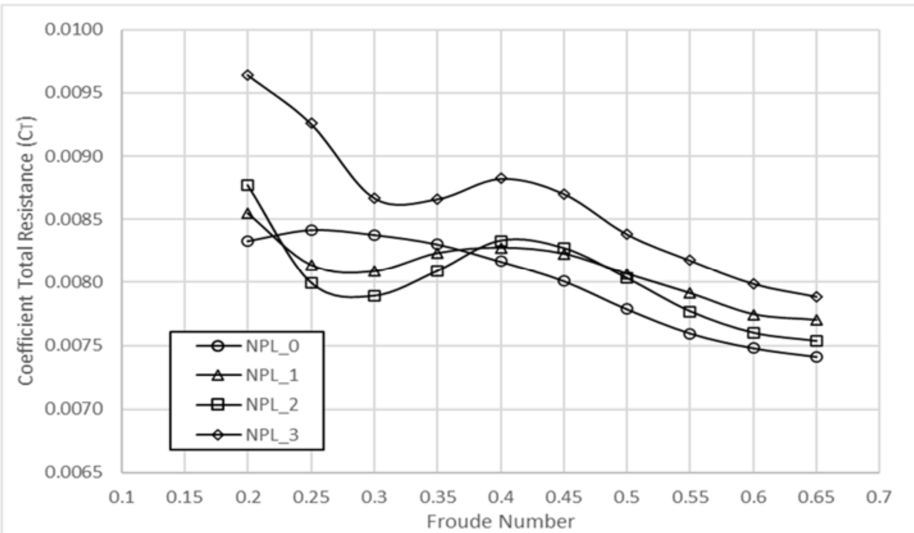

Figure 5 Coefficient total resistance of NPL Hull with Bow variations

NPL model 0 provides the smallest resistance at low speeds (Fr-0.2) this is due to the smaller wetted surface area so that at this speed, the Model 0 hull does not cause significant friction. In addition, in this condition the movement of Model 0 does not cause much waves on the water surface as shown in Figure 6

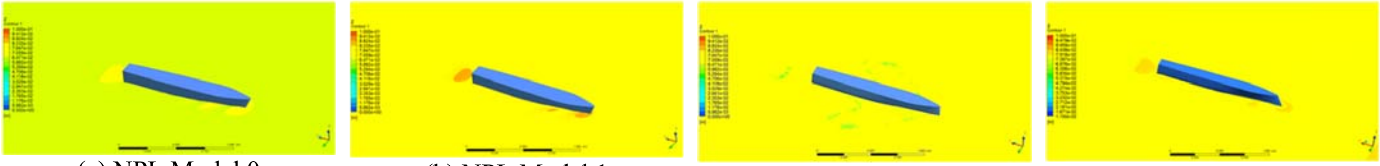

(a) NPL Model 0 (b) NPL Model 1 (c) NPL Model 2 (d) NPL Model 3

Figure 6 Wave elevation at low speed (Fr=0.2)

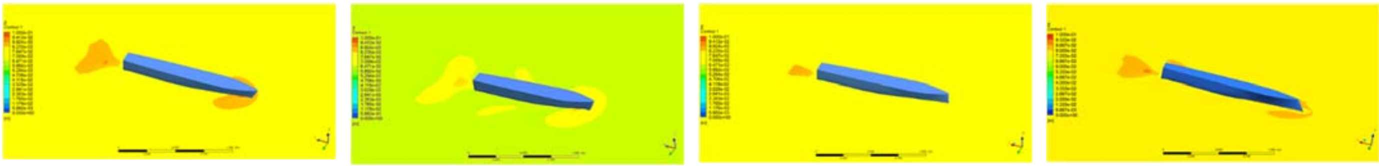

(a) NPL Model 0 (b) NPL Model 1 (c) NPL Model 2 (d) NPL Model 3

Figure 7 Wave elevation at medium speed (Fr=0.3)

At medium speed (Fr=0.3), NPL Models 1 and 2 have low resistance compared to other models. As shown in Figure 7, it shows that in both models the wave effect caused by the movement of the model is smaller than the other, this causes the two models to have smaller resistance than the other models.

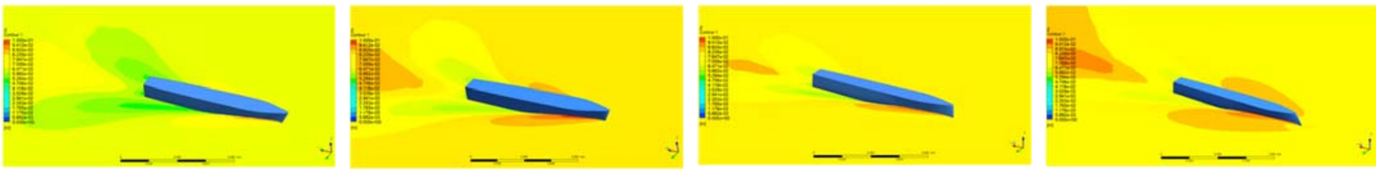

(a) NPL Model 0 (b) NPL Model 1 (c) NPL Model 2 (d) NPL Model 3

Figure Wave elevation at high speed (Fr=0.65)

NPL Model 0 has a smaller dominant resistance than the other models. Figure 8 shows the effect of surface water waves caused by the movement of the NPL Model 1 which is the least compared to the others. At high speed (Fr=0.65) the effect of waves due to the movement of the ship (wave resistance) is very dominant to the total resistance of the ship

V. CONCLUSION

The effects of various bow for NPL hull was investigated by CFD analysis. The following conclusions can be drawn from the the approach that the resistances of the NPL using the model 1 design is the best model for low (Fr=0.2) and high speed (Fr>0.4) and using NPL model 1 and 3 are the best for medium speed (Fr=0.25 to 0.35). CFD plays a very important role in the prediction of ship resistance

ACKNOWLEDGMENT

The author would like to thank Pattimura University for providing access to the Ship Modeling Laboratory so that this paper can be completed properly

REFERENCES

[1] J. S. Carlton, "Chapter 12 - Resistance and Propulsion," in *Marine Propellers and Propulsion (Fourth Edition)*, J. S. Carlton, Ed. Butterworth-Heinemann, 2019, pp. 313–365. doi: 10.1016/B978-0-08-100366-4.00012-2.

[2] Y. Liu, L. S. Zhang, L. P. Sun, and B. Li, “Numerical study on effects of buffer bulbous bow structure in collisions,” in *Recent Advances in Structural Integrity Analysis - Proceedings of the International Congress (APCF/SIF-2014)*, L. Ye, Ed. Oxford: Woodhead Publishing, 2014, pp. 168–172. doi: 10.1533/9780081002254.168.

[3] J. L. Gelling, “the Axe Bow: the shape of Ships to Come,” 2006.

[4] T. Buckley, “The Axe Factor : Damen dan Amels Take a Bow,” *Yatch Rep.*, no. 111, 2010.

[5] Damen Shipyard, “P511-Guardião: Damen Shipyard’s first full axe-bow patrol vessel delivered to Cape Uerdean coast guard,” *Marit. Holl.*, 2012.

[6] W. Seok, G. H. Kim, J. Seo, and S. H. Rhee, “Application of the design of experiments and computational fluid dynamics to bow design improvement,” *J. Mar. Sci. Eng.*, 2019, doi: 10.3390/jmse7070226.

[7] T.-H. Le *et al.*, “Numerical investigation on the effect of trim on ship resistance by RANSE method,” *Appl. Ocean Res.*, vol. 111, p. 102642, Jun. 2021, doi: 10.1016/j.apor.2021.102642.

[8] F. R. Menter, M. Kuntz, and R. Langtry, “Ten Years of Industrial Experience with the SST Turbulence Model,” in *4th Internal Symposium, Turbulence, heat and mass transfer*, New York, Wallingford, 2003, pp. 625–632.

[9] F. R. Menter, “Zonal two equation κ-$ømega$ turbulence models for aerodynamic flows,” 1993.

[10] F. R. Menter, “Two-equation eddy-viscosity turbulence models for engineering applications,” *AIAA J.*, vol. 32, no. 8, pp. 1598–1605, Aug. 1994, doi: 10.2514/3.12149.

[11] J. E. Bardina, P. G. Huang, and T. J. Coakley, “Turbulence Modeling Validation, Testing, and Development,” *Nasa Tech. Memo.*, 1997, doi: 10.2514/6.1997-2121.

[12] I. K. A. P. Utama, Sutiyo, and I. K. Suastika, “Experimental and Numerical Investigation into the Effect of the Axe-Bow on the Drag Reduction of a Trimaran Configuration,” *Int. J. Technol.*, vol. 12, no. 3, pp. 527–538, Jul. 2021, doi: 10.14716/ijtech.v12i3.4659.